Space: Science & Technology
A SCIENCE PARTNER JOURNAL

RESEARCH ARTICLE

Dynamics and FNTSM Control of Spacecraft with a Film Capture Pocket System

Zhuoran Huang[1], Chao Tang[1], Qiang Yu[2], Mohamed Shehata[3], and Cheng Wei[1]*

[1]School of Astronautics, Harbin Institute of Technology, Harbin, China. [2]Beijing Institute of control engineering, China Academy of Space Technology, Beijing, China. [3]Mechanical Engineering Department, Benha Faculty of Engineering, Benha University, Benha, Egypt.

*Address correspondence to: weicheng@hit.edu.cn

Citation: Huang Z, Tang C, Yu Q, Khaliel MSS, Wei C. Dynamics and FNTSM Control of Spacecraft with a Film Capture Pocket System. *Space Sci. Technol.* 2023;3:Article 0079. https://doi.org/10.34133/space.0079

Submitted 20 June 2023
Accepted 5 September 2023
Published 1 November 2023

To solve the problem of space debris, a film capture pocket system is designed in this paper. The film capture pocket is more flexible and reliable, compared with the space rope net. The film capture pocket system contains many flexible structures that are prone to large deformation and vibration during movement. The deformation causes large disturbances to the service spacecraft. It is necessary to establish an accurate rigid-flexible coupling dynamic model for quantitative analysis of disturbances. First, a film dynamic model is developed using high-order absolute nodal coordinate formulation. Second, an attitude tracking control law is designed by using the fast nonsingular terminal sliding mode controller and fixed time dilation observer (FxESO). Finally, combining dynamics and control principles, a virtual prototype of spacecraft with film capture pocket system is established. The simulation results show that higher-order absolute nodal coordinate formulation elements have better convergence, compared to ABAQUS finite element analysis. Meanwhile, the dynamic model simulates the deformation and vibration states of large flexible structures, during the spacecraft maneuver. The FxESO can estimate and compensate the complex disturbance. The error under fast nonsingular terminal sliding mode + FxESO control law converge more rapidly than the nonsingular terminal sliding mode + expansion observer control law. The final spacecraft attitude tracking error is about 10^{-4}, indicating the effectiveness of the controller.

Introduction

With the human space activities increasing, the space environment problems are becoming more and more serious [1]. Flexible capture technology represented by space rope net is considered as a promising space debris active removal technology [2]. There are many advantages of traditional rope net capture system, such as simple structure, light weight, large capture envelope, and high error tolerance of capture control. However, the shape of the net surface is difficult to maintain for a long time as shown in Fig. 1. If the rope net is not unfolded at the proper angle and speed, the net will be difficult to fully deploy, and the capture area of the rope net will be reduced. During the unfolding process of the rope net, there is no regular net surface pattern, and there is constant contact friction between multiple ropes. Because of the contact friction between the ropes, the rope net system is prone to self-tangling, as shown in Fig. 2. The self-tangling of the rope net causes the loss of kinetic energy in the unfolding process, which prevents the rope net from unfolding or reduces the retention time of the rope net in the effective capture domain. The film surface can be folded and unfolded along the creases, and the unfolding process has a regular shape. Therefore, the film surfaces are not prone to self-tangling. In this paper, a capture pocket system with film surfaces as the main structure is proposed. The system is an umbrella shaped structure, which consists 8 film surfaces as the main structure and 8 large flexible rods as supporting structure. The size of the target captured by the film capture pocket system is not limited by the net diameter, so the system is more suitable for capturing mall-sized and multiple targets. In this paper, the dynamic modeling and attitude control of film pocket capture system are studied.

The film pocket capture system is a multiflexible body system. In the multibody system, the large range movement of the rigid spacecraft is coupled with the large nonlinear deformation of the flexible capture device. The classical finite element method is generally under the small deformation assumption to derive the reference equations in floating coordinates, so the equations are only suitable for small deformation cases. According to the generalized coordinates, the kinematic description methods used for large rotation and deformation systems mainly include absolute nodal coordinate formulation (ANCF) [3,4], geometrically exact method (GME) [5,6], iso-geometric analysis (IGA) [7,8], etc. The GME method uses node displacement vectors and rotation parameters as generalized coordinates. Compared with the ANCF, the GME method requires a rational parameterization to describe finite rotations to avoid singularities in the rotation parameters. In addition, the GME method interpolates the displacement and rotation fields separately, resulting in 2 different geometric shapes of spatial curves and different rigid body displacements. Some studies [9,10] also point out that for large deformation problems, rotation angle interpolation will reduce the accuracy of strain energy and inertial

The working process of the system is mainly in 3 stages, as shown in Fig. 4. First, the spacecraft system is driven by the high thrust engine to approach the captured target. Then, inflatable flexible joints are inflated to envelop the target. Finally, the service spacecraft actively maneuvers to drag the captured target into the graveyard orbit.

Dynamics of the spacecraft with film capture pocket system

Dynamics of the film surfaces

Kinematics of the film surface

Both the ANCF method and the IGA method discard the use of node angles as generalized coordinates, which can avoid the difficulties of finite rotation parameterization and interpolation in the GME method. However, for the IGA method, the control points are always not within the element. The shape of the film surface in the capture structure is relatively regular, and there are many constraints between the film surface and the flexible rod. Therefore, the ANCF method is more suitable for the modeling analysis in this article. The kinematics of the film surface is described using ANCF, as shown in Fig. 5. Each high-order ANCF element is composed of 8 nodes. The element has 24 node coordinate vectors and 72 degrees of freedom. The global vector $\boldsymbol{ri}$ of a material point $\boldsymbol{n} = [\boldsymbol{xi}\ \ \boldsymbol{yi}\ \ \boldsymbol{zi}]^{\mathrm{T}}$ in the shell element $\boldsymbol{i}$ is defined as:

$$\boldsymbol{r}^i = \boldsymbol{r}^i{}_m\left(x^i, y^i\right) + z^i \frac{\partial \boldsymbol{r}^i}{\partial z^i}\left(x^i, y^i\right) + \frac{1}{2} z^{i2} \frac{\partial \boldsymbol{r}^i}{\partial z^{i2}}\left(x^i, y^i\right) \quad (1)$$

where $\boldsymbol{r}_{\boldsymbol{m}}^{\boldsymbol{i}}\left(x^i, y^i\right)$ is the global position vector in the middle surface. The interpolation representation of the global position vector $\boldsymbol{ri}$ using polynomials is as follows:

$$\boldsymbol{r}^i = \begin{bmatrix} r_1^i \\ r_2^i \\ r_3^i \end{bmatrix} = \begin{bmatrix} \boldsymbol{\Phi}_1(x,y) + z^i \boldsymbol{\Phi}_2(x,y) + 0.5 z^{i2} \boldsymbol{\Phi}_3(x,y) \\ \boldsymbol{\Phi}_4(x,y) + z^i \boldsymbol{\Phi}_5(x,y) + 0.5 z^{i2} \boldsymbol{\Phi}_6(x,y) \\ \boldsymbol{\Phi}_7(x,y) + z^i \boldsymbol{\Phi}_8(x,y) + 0.5 z^{i2} \boldsymbol{\Phi}_9(x,y) \end{bmatrix} \quad (2)$$

where $\boldsymbol{\Phi}_i(x,y) = a_{i0} + a_{i1}x^i + a_{i2}y^i + a_{i3}x^i y^i + a_{i4}x^{i2} + a_{i5}y^{i2} + a_{i6}x^{i2}y^i + a_{i7}x^i y^{i2}$ is a interpolation polynomial with the highest degree term of 3.

The element nodal coordinate vector e^i is defined as

$$\boldsymbol{e}^i = \left[\left(\boldsymbol{e}_p^i\right)^{\mathrm{T}} \ \left(\boldsymbol{e}_{pz}^i\right)^{\mathrm{T}} \ \left(\boldsymbol{e}_{pzz}^i\right)^{\mathrm{T}}\right]^{\mathrm{T}} \quad (3)$$

where $\boldsymbol{e}_{\boldsymbol{p}}^{\boldsymbol{i}}$ represents the position coordinates of element nodes. For node k (k = 1, 2, …, 8) in shell element i, the definitions are

$$\boldsymbol{e}_p^i = \left[\boldsymbol{e}_p^{i1\mathrm{T}} \ \boldsymbol{e}_p^{i2\mathrm{T}} \ \boldsymbol{e}_p^{i3\mathrm{T}} \ \boldsymbol{e}_p^{i4\mathrm{T}} \ \boldsymbol{e}_p^{i5\mathrm{T}} \ \boldsymbol{e}_p^{i6\mathrm{T}} \ \boldsymbol{e}_p^{i7\mathrm{T}} \ \boldsymbol{e}_p^{i8\mathrm{T}}\right]^{\mathrm{T}} \quad (4)$$

$\boldsymbol{e}_{pz}^i$ and $\boldsymbol{e}_{pz}^i$ are the gradient vectors, defined as $\boldsymbol{e}_{pz}^{ik} = \partial \boldsymbol{e}^{ik} / \partial z^i$ and $\boldsymbol{e}_{pzz}^{ik} = \partial \boldsymbol{e}^{ik} / \partial z^{i2}$.

The shape function matrix $\boldsymbol{S}^i(x^i, y^i, z^i)$ is defined as

$$\boldsymbol{S}^i = \left[\boldsymbol{S}_m^i\left(x^i, y^i\right) \ \ z^i \boldsymbol{S}_m^i\left(x^i, y^i\right) \ \ 0.5 z^{i2} \boldsymbol{S}_m^i\left(x^i, y^i\right)\right] \quad (5)$$

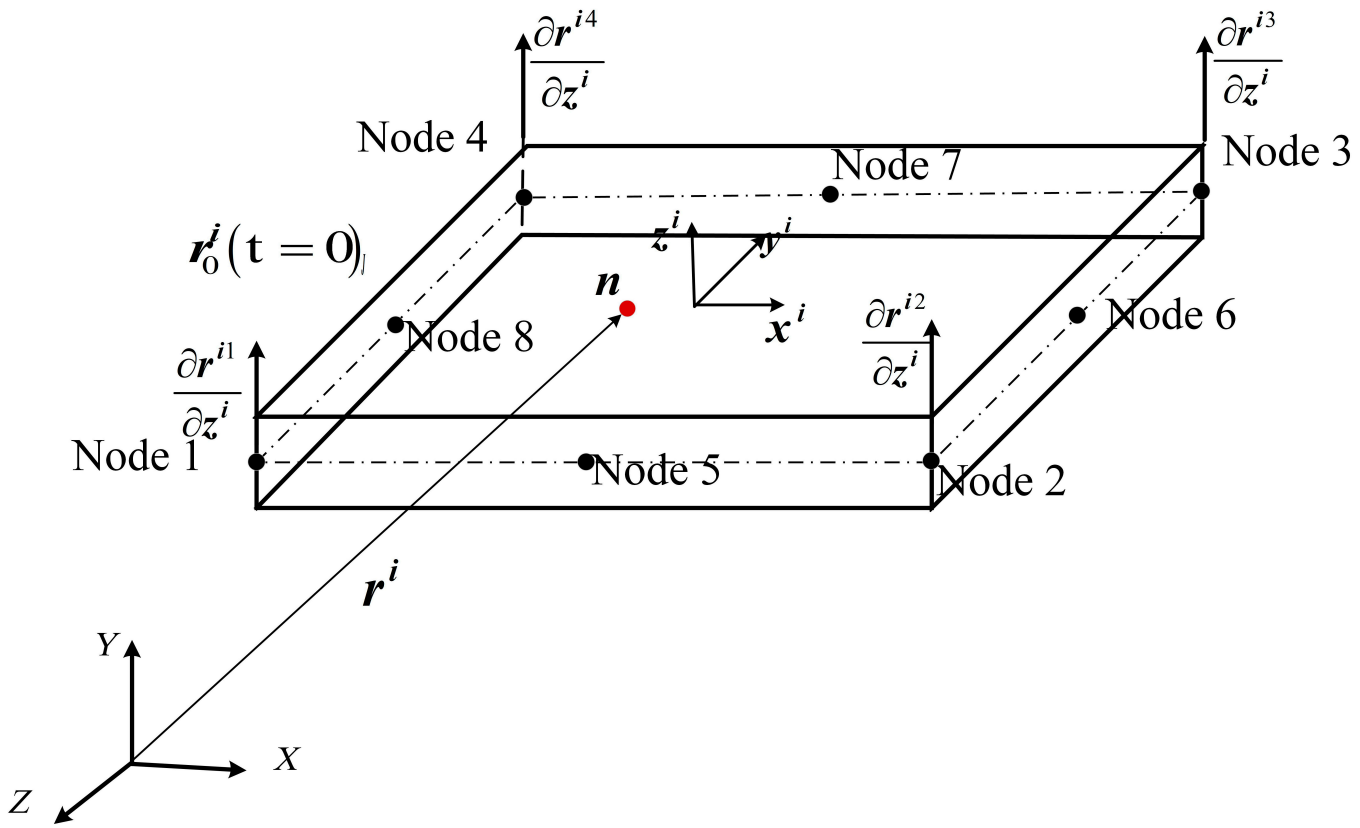

Fig. 5. Kinematics of ANCF element.

$$\boldsymbol{S}_m^i = \left[S_1^i\boldsymbol{I}\ \ S_2^i\boldsymbol{I}\ \ S_3^i\boldsymbol{I}\ \ S_4^i\boldsymbol{I}\ \ S_5^i\boldsymbol{I}\ \ S_6^i\boldsymbol{I}\ \ S_7^i\boldsymbol{I}\ \ S_8^i\boldsymbol{I}\right] \tag{6}$$

$$\begin{gathered} S_1^i = -\frac{1}{4}\left(-1+\xi^i\right)\left(-1+\eta^i\right)\left(1+\xi^i+\eta^i\right), \quad S_2^i = -\frac{1}{4}\left(1+\xi^i\right)\left(-1+\eta^i\right)\left(-1+\xi^i-\eta^i\right) \\ S_3^i = \frac{1}{4}\left(1+\xi^i\right)\left(1+\eta^i\right)\left(-1+\xi^i+\eta^i\right), \quad S_4^i = \frac{1}{4}\left(-1+\xi^i\right)\left(1+\eta^i\right)\left(1+\xi^i-\eta^i\right) \\ S_5^i = \frac{1}{2}\left(-1+\xi^i\right)\left(1+\xi^i\right)\left(-1+\eta^i\right), S_6^i = -\frac{1}{2}\left(1+\xi^i\right)\left(1+\eta^i\right)\left(-1+\eta^i\right) \\ S_7^i = -\frac{1}{2}\left(-1+\xi^i\right)\left(1+\xi^i\right)\left(1+\eta^i\right), S_8^i = \frac{1}{2}\left(-1+\xi^i\right)\left(1+\eta^i\right)\left(-1+\eta^i\right) \end{gathered} \tag{7}$$

where $\xi^i = 2x^i/l^i$, $\eta^i = 2y^i/w^i$, and l^i and w^i are the length of the film element along the ***xi*** and ***yi*** axes.

Refer to the research of Yamashita et al. [24] , the Green–Lagrange strain tensor $\boldsymbol{\varepsilon}^i$ of a material point n in element i is defined as follows:

$$\boldsymbol{\varepsilon}^i = \frac{1}{2}\left(\left(\boldsymbol{J}^i\right)^{\mathrm{T}}\boldsymbol{J}^i - \boldsymbol{I}\right) \tag{8}$$

where J^i is the global position vector gradient tensor. Using the initial configuration as the reference configuration, the global coordinates $\boldsymbol{X}^i$ under the reference configuration satisfies $\boldsymbol{X}^i = \boldsymbol{r}^i\left(x_0^i, y_0^i, z_0^i, t=0\right)$. Then, J^i can be written as follows:

$$\boldsymbol{J} = \frac{\partial \boldsymbol{r}^i\left(x^i, y^i, z^i t\right)}{\partial \boldsymbol{r}_0^i\left(x_0^i, y_0^i, z_0^i, t=0\right)} = \frac{\partial \boldsymbol{r}^i}{\partial \boldsymbol{X}^i}\frac{\partial \boldsymbol{X}^i}{\partial \boldsymbol{X}^i} = \tilde{\boldsymbol{J}}\bar{\boldsymbol{J}}^{-1} \tag{9}$$

$$\tilde{\boldsymbol{J}} = \frac{\partial \boldsymbol{r}^i}{\partial \boldsymbol{x}^i} = \left[\begin{array}{ccc} \boldsymbol{r}_x^i & \boldsymbol{r}_y^i & \boldsymbol{r}_z^i \end{array}\right] = \left[\begin{array}{ccc} \boldsymbol{S}_x^i\boldsymbol{e}^i(t) & \boldsymbol{S}_y^i\boldsymbol{e}^i(t) & \boldsymbol{S}_z^i\boldsymbol{e}^i(t) \end{array}\right] \tag{10}$$

$$\bar{\boldsymbol{J}} = \frac{\partial \boldsymbol{X}^i}{\partial \boldsymbol{x}^i} = \left[\begin{array}{ccc} \boldsymbol{S}_x^i\boldsymbol{e}^i(t=0) & \boldsymbol{S}_y^i\boldsymbol{e}^i(t=0) & \boldsymbol{S}_z^i\boldsymbol{e}^i(t=0) \end{array}\right] \tag{11}$$

Then, $\boldsymbol{\varepsilon}^i$ can be written as follows:

$$\begin{aligned} \boldsymbol{\varepsilon}^i &= \frac{1}{2}\left(\left(\boldsymbol{J}^i\right)^{\mathrm{T}}\boldsymbol{J}^i - \boldsymbol{I}\right) = \frac{1}{2}\left(\left(\tilde{\boldsymbol{J}}^i\left(\bar{\boldsymbol{J}}^i\right)^{-1}\right)^{\mathrm{T}}\tilde{\boldsymbol{J}}^i\left(\bar{\boldsymbol{J}}^i\right)^{-1} - \boldsymbol{I}\right) \\ &= \frac{1}{2}\bar{\boldsymbol{J}}^{-\mathrm{T}}\left(\left(\tilde{\boldsymbol{J}}^i\right)^{\mathrm{T}}\tilde{\boldsymbol{J}}^i - \left(\bar{\boldsymbol{J}}^i\right)^{\mathrm{T}}\bar{\boldsymbol{J}}^i\right)\left(\bar{\boldsymbol{J}}^i\right)^{-1} \\ &= \left(\bar{\boldsymbol{J}}^i\right)^{-\mathrm{T}}\hat{\boldsymbol{\varepsilon}}^i\left(\bar{\boldsymbol{J}}^i\right)^{-1} \end{aligned} \tag{12}$$

where $\hat{\boldsymbol{\varepsilon}}^i = \frac{1}{2}\left(\tilde{\boldsymbol{J}}^{\mathrm{T}}\tilde{\boldsymbol{J}} - \bar{\boldsymbol{J}}^{\mathrm{T}}\bar{\boldsymbol{J}}\right)$ is the covariant strain tensor.

$\boldsymbol{\varepsilon}_v^i$ is a symmetric matrix with 6 variables, $\boldsymbol{\varepsilon}_{xx}^i\ \boldsymbol{\varepsilon}_{yy}^i\ \gamma_{xy}^i\ \boldsymbol{\varepsilon}_{zz}^i\ \gamma_{xz}^i\ \gamma_{yz}^i$. The engineering strain vector about $\boldsymbol{\varepsilon}_v^i$ can be defined as follows:

$$\boldsymbol{\varepsilon}_v^i = \left[\begin{array}{cccccc} \boldsymbol{\varepsilon}_{xx}^i & \boldsymbol{\varepsilon}_{yy}^i & \boldsymbol{\varepsilon}_{zz}^i & 2\gamma_{xy}^i & 2\gamma_{xz}^i & 2\gamma_{yz}^i \end{array}\right]^{\mathrm{T}} \tag{13}$$

Equations of element motion

According to the principle of virtual work in dynamics, the generalized elastic force virtual work can be written as

$$\delta W_e^i = -\left|\bar{J}\right|\int_{V_0}\boldsymbol{\sigma}^i : \delta\boldsymbol{\varepsilon}^i \mathrm{d}V_0 = -\left|\bar{J}\right|\int_{V_0}\left(\boldsymbol{E}_e\boldsymbol{\varepsilon}_v^i\right)^{\mathrm{T}}\frac{\partial \boldsymbol{\varepsilon}_v^i}{\partial \boldsymbol{e}^i}\,\mathrm{d}V_0\delta\boldsymbol{e}^i = -\boldsymbol{Q}_e^i\delta\boldsymbol{e}^i \tag{14}$$

where $\boldsymbol{Q}_e^i = -\left|\bar{J}\right|\int_{V_0}\left(\boldsymbol{E}\boldsymbol{\varepsilon}_v^i\right)^{\mathrm{T}}\frac{\partial \boldsymbol{\varepsilon}_v^i}{\partial \boldsymbol{e}^i}\,\mathrm{d}V_0$ is the generalized elastic force vector, V_0 is the reference configuration volume, $\boldsymbol{E}_e$ is the matrix of elastic coefficients, and, for anisotropic linearly elastic material, $\boldsymbol{E}_e$ is defined as follows

$$\boldsymbol{E}_e = \left[\begin{array}{cccccc} \frac{E(1-\nu)}{1-\nu-2\nu^2} & \frac{E\nu}{1-\nu-2\nu^2} & \frac{E\nu}{1-\nu-2\nu^2} & 0 & 0 & 0 \\ \frac{E\nu}{1-\nu-2\nu^2} & \frac{E(1-\nu)}{1-\nu-2\nu^2} & \frac{E\nu}{1-\nu-2\nu^2} & 0 & 0 & 0 \\ \frac{E\nu}{1-\nu-2\nu^2} & \frac{E\nu}{1-\nu-2\nu^2} & \frac{E(1-\nu)}{1-\nu-2\nu^2} & 0 & 0 & 0 \\ 0 & 0 & 0 & 2G & 0 & 0 \\ 0 & 0 & 0 & 0 & 2G & 0 \\ 0 & 0 & 0 & 0 & 0 & 2G \end{array}\right] \tag{15}$$

where $G = \frac{E}{2(1+\nu)}$ is called the shear modulus, E is Young's modulus, and ν is Poisson's ratio.

The generalized inertial force virtual work can be written as

$$\delta W_I^i = \rho_0\left|\tilde{J}_0\right|\int_{V_0}\ddot{\boldsymbol{r}}^{i\mathrm{T}}\delta\boldsymbol{r}^i\,\mathrm{d}V_0 = \left(\rho_0\left|\bar{J}\right|\int_{V_0}\boldsymbol{S}^{i\mathrm{T}}\boldsymbol{S}^i\ddot{\boldsymbol{e}}^i\,\mathrm{d}V_0\right)\delta\boldsymbol{e}^i = \boldsymbol{Q}_I^i\delta\boldsymbol{e}^i = \boldsymbol{M}\ddot{\boldsymbol{e}}^i\delta\boldsymbol{e}^i \tag{16}$$

where $\boldsymbol{Q}_I^i = \boldsymbol{M}\ddot{\boldsymbol{e}}^i$ is the generalized inertial force vector, $\boldsymbol{M} = \rho_0\left|\bar{J}\right|\int_{V_0^i}\boldsymbol{S}^{i\mathrm{T}}\boldsymbol{S}^i\,\mathrm{d}V_0^i$ is the generalized mass matrix, and ρ_0 is the material density at the reference configuration evaluated.

The generalized external force virtual work can be written as

$$\delta W_f^i = \left|\bar{J}\right|\int_{V_0^i}\boldsymbol{F}^{i\mathrm{T}}\delta\boldsymbol{r}^i dV_0^i = \left|\bar{J}\right|\int_{V_0^i}\boldsymbol{F}^{i\mathrm{T}}\left(\frac{\partial \boldsymbol{r}^i}{\partial \boldsymbol{e}^i}\right)^{\mathrm{T}}dV_0^i\delta\boldsymbol{e}^i = \boldsymbol{Q}_f^i\delta\boldsymbol{e}^i \tag{17}$$

where $\boldsymbol{Q}_f^i = \left|\bar{J}\right|\int_{V_0^i}\left(\frac{\partial \boldsymbol{r}^i}{\partial \boldsymbol{e}^i}\right)^{T}\boldsymbol{F}^i dV_0^i$ is the generalized external force vector and $\boldsymbol{F}^i$ is the external force.

On the basis of Eqs. 14, 16, and 17, the equations of the element i can be expressed as

$$\delta W_I^i - \delta W_f^i - \delta W_e^i = 0 \tag{18}$$

$$\boldsymbol{M}\ddot{\boldsymbol{e}}^i\delta\boldsymbol{e}^i - \boldsymbol{Q}_f^i\delta\boldsymbol{e}^i + \boldsymbol{Q}_e^i\delta\boldsymbol{e}^i = 0 \tag{19}$$

Finally, the equation of the element i is derived as

$$\boldsymbol{M}\ddot{\boldsymbol{e}}^i - \boldsymbol{Q}_k^i + \boldsymbol{Q}_e^i = 0 \tag{20}$$

Attitude dynamics of spacecraft system

The attitude dynamic equation of the spacecraft with external disturbances $\boldsymbol{d}$ can be expressed as follows [25]

$$\boldsymbol{J}_{\boldsymbol{R}}\dot{\boldsymbol{\omega}} + \boldsymbol{\omega}^*\boldsymbol{J}_{\boldsymbol{R}}\boldsymbol{\omega} = \boldsymbol{u} + \boldsymbol{d} \tag{21}$$

where $\boldsymbol{u}$ is the controller of the spacecraft, $\boldsymbol{\omega}$ is angular velocity, and $(\cdot)^*$ means $(\cdot)\times$. The unit quaternion $\boldsymbol{q} = \left[\begin{array}{cc} q_0 & \tilde{\boldsymbol{q}}^{\mathrm{T}} \end{array}\right]^{\mathrm{T}}$ corresponds to the body frame attitude of the spacecraft. q_0 is

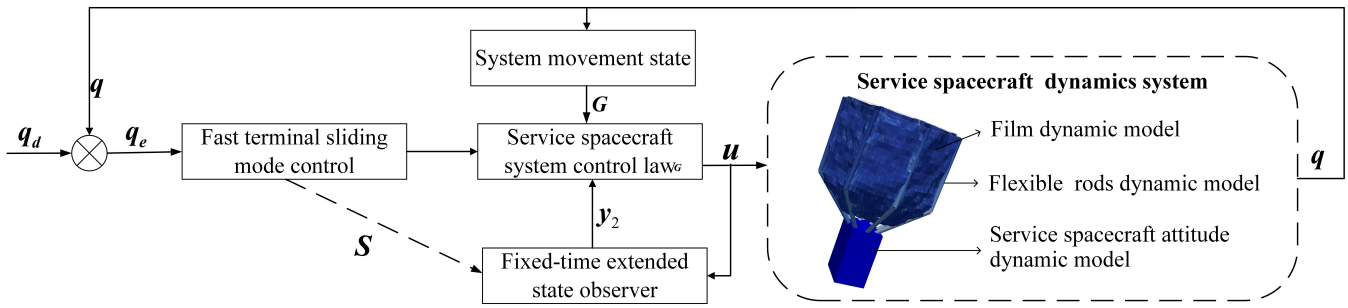

Fig. 10. Virtual prototype of the spacecraft with film capture pocket system.

Table 1. Controller parameters of the system

Parameter name	Value
FNTSM parameters	$k_1 = 10, k_2 = 2, \alpha_1 = \frac{11}{5}, \alpha_2 = \frac{11}{19}$
FxESO parameters	$\beta_1 = 4, \beta_2 = 2, \gamma_1 = 15, \gamma_2 = 7.5, \eta = 15$
	$o_1 = 0.99, \zeta_1 = 1.01, \alpha_3 = \frac{11}{5}, \alpha_4 = \frac{11}{19}$
Initial attitude quaternion $q_{t=0}$	$[1\ 0\ 0\ 0]^{\mathrm{T}}$
desired attitude quaternion q_d	$[0.9659\ \ 0.1494\ \ 0.1494\ \ -0.1494]^{\mathrm{T}}$

where $\iota_1 = (2-\alpha_2)\psi^{\alpha_2^{-1}}$, $\iota_1 = (\alpha_2 - 1)\,\psi^{\alpha_2 - 1.5}$.

Proof:

Taking the Lyapunov function V as follows:

$$V_1 = \frac{1}{2}\tilde{\boldsymbol{q}}_e^{\mathrm{T}}\tilde{\boldsymbol{q}}_e \tag{26}$$

The derivative of $\boldsymbol{V}$ can be derived as follows:

$$\dot{V}_1 = \tilde{\boldsymbol{q}}_e^{\mathrm{T}}\dot{\tilde{\boldsymbol{q}}}_e = \boldsymbol{q}_e^{\mathrm{T}} \bullet \frac{1}{2} \bullet \varphi(\boldsymbol{q}_e)\boldsymbol{\omega}_e \tag{27}$$

When $S = 0$, the Eq. 24 can be derived as follows:

$$\boldsymbol{\omega}_e = -\left(2k_1\varphi^{-1}(\boldsymbol{q}_e)\boldsymbol{sig}^{\alpha_1}(\tilde{\boldsymbol{q}}_e) + 2k_2\varphi^{-1}(\boldsymbol{q}_e)\mathrm{sig}^{\alpha_2}(\tilde{\boldsymbol{q}}_e)\right) \tag{28}$$

According to Eqs. 22 and 28, $\dot{V}$ can be further derived as follows:

$$\begin{aligned}\dot{V}_1 &= -\tilde{\boldsymbol{q}}_e^{\mathrm{T}} \bullet \frac{1}{2} \bullet \varphi(\boldsymbol{q}_e) \bullet \left(2k_1\varphi^{-1}(\boldsymbol{q}_e)\mathbf{sig}^{\alpha_1}(\tilde{\boldsymbol{q}}_e) + 2k_2\varphi^{-1}(\boldsymbol{q}_e)\mathrm{sig}^{\alpha_2}(\tilde{\boldsymbol{q}}_e)\right) \\ &= -\tilde{\boldsymbol{q}}_e^{\mathrm{T}}\left(k_1\mathbf{sig}^{\alpha_1}(\tilde{\boldsymbol{q}}_e) + k_2\mathbf{sig}^{\alpha_2}(\tilde{\boldsymbol{q}}_e)\right) \\ &\le -\left(k_1\sum_{i=1}^{3}(\tilde{q}_{ei}^2)^{\frac{\alpha_1+1}{2}} + k_2\sum_{i=1}^{3}(\tilde{q}_{ei}^2)^{\frac{\alpha_2+1}{2}}\right)\end{aligned} \tag{29}$$

On the basis of [27], it can be proved that

$$\sum_{i=1}^{3}(\tilde{q}_{ei}^2)^{\frac{\alpha_1+1}{2}} \ge 3^{\frac{1-\alpha_1}{2}}\left(\sum_{i=1}^{3}\tilde{q}_{ei}^2\right)^{\frac{\alpha_1+1}{2}},\ \sum_{i=1}^{3}(\tilde{q}_{ei}^2)^{\frac{\alpha_2+1}{2}} \ge 3^{\frac{1-\alpha_2}{2}}\left(\sum_{i=1}^{3}\tilde{q}_{ei}^2\right)^{\frac{\alpha_2+1}{2}} \tag{30}$$

Then, $\dot{V}$ is written as follows:

$$\begin{aligned}\dot{V}_1 &\le -k_1 3^{\frac{1-\alpha_1}{2}}\left(\sum_{i=1}^{3}\tilde{q}_{ei}^2\right)^{\frac{\alpha_1+1}{2}} - k_2 3^{\frac{1-\alpha_2}{2}}\left(\sum_{i=1}^{3}\tilde{q}_{ei}^2\right)^{\frac{\alpha_2+1}{2}} \\ &\le -k_1 3^{\frac{1-\alpha_1}{2}} V_1^{\frac{\alpha_1+1}{2}} - k_2 3^{\frac{1-\alpha_2}{2}} V_1^{\frac{\alpha_2+1}{2}}\end{aligned} \tag{31}$$

Then, it can be proved that $\tilde{\boldsymbol{q}}_e = \boldsymbol{0}, \boldsymbol{\omega}_e = \boldsymbol{0}$, and $q_{e0} = \pm 1$, within the limited time $t_0 \to T_0$.

Design of the fixed time extended state observer

According to Eq. 24, the derivative of S_F can be written as:

$$\begin{aligned}\dot{\boldsymbol{S}}_F = \dot{\omega}_e &+ 2\alpha_1 k_1\varphi^{-1}(\boldsymbol{q}_e)\mathrm{diag}\left\{|\tilde{\boldsymbol{q}}_{ei}|^{\alpha_1-1}\right\}\dot{\tilde{\boldsymbol{q}}}_e + 2\alpha_2 k_2\varphi^{-1}(\boldsymbol{q}_e)\mathrm{diag}\left\{|\tilde{\boldsymbol{q}}_{ei}|^{\alpha_2-1}\right\} \\ &+ 2k_1\dot{\varphi}^{-1}(\boldsymbol{q}_e)sig^{\alpha_1}(\tilde{\boldsymbol{q}}_e) + 2k_2\dot{\varphi}^{-1}(\boldsymbol{q}_e)sig^{\alpha_2}(\tilde{\boldsymbol{q}}_e)\end{aligned} \tag{32}$$

Considering the uncertainty of spacecraft inertia with film bag capture system, the spacecraft inertia can be written as $J_R = J_{R0} + \Delta J_R$, where J_{R0} is the known inertia matrix and ΔJ_R is the uncertainty inertia matrix of spacecraft system. It can be obtained as follows:

$$\begin{aligned}J_{R0}\dot{S}_F = (J_R - \Delta J_R)\Big(&\dot{\omega}_e + 2\alpha_1 k_1\varphi^{-1}(\boldsymbol{q}_e)\mathrm{diag}\left\{|\tilde{\boldsymbol{q}}_{ei}|^{\alpha_1-1}\right\}\dot{\tilde{\boldsymbol{q}}}_e + 2\alpha_2 k_2\varphi^{-1}(\boldsymbol{q}_e)\mathrm{diag}\left\{|\tilde{\boldsymbol{q}}_{ei}|^{\alpha_2-1}\right\} \\ &+ 2k_1\dot{\varphi}^{-1}(\boldsymbol{q}_e)sig^{\alpha_1}(\tilde{\boldsymbol{q}}_e) + 2k_2\dot{\varphi}^{-1}(\boldsymbol{q}_e)sig^{\alpha_2}(\tilde{\boldsymbol{q}}_e)\Big)\end{aligned} \tag{33}$$

Substitute the system dynamic equation Eq. 23 into Eq. 33 as follows:

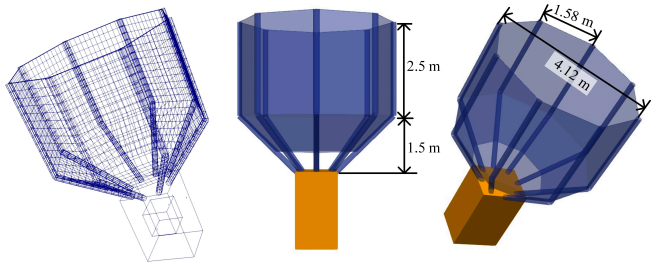

Fig. 11. Size of the film capture pocket system.

Table 2. Dynamic parameters of the service spacecraft

Parameter name	Service spacecraft
Mass (kg)	110
J_{ROx} (kg·m^2)	384
J_{ROy} (kg·m^2)	596
J_{ROz} (kg·m^2)	398

Table 3. Material properties of film surface and flexible rods

Parameter name	Film surface	Flexible rods
Density (kg/m^3)	1430	164
Poisson ratio	0.3	0.3
Modulus of elasticity (MPa)	3.2	750

$$\begin{aligned}J_0\dot{S}_F=&-(\omega_e+A(q_e)\omega_d)^{*}J_{R0}(\omega_e+A(q_e)\omega_d)+J_{R0}(\omega_e{}^{*}A(q_e)\omega_d-A(q_e)\dot{\omega}_d)\\&+\alpha_1k_1J_{R0}\varphi^{-1}\mathrm{diag}\left\{|\tilde{q}_{ei}|^{\alpha_1-1}\right\}\varphi\omega_e+\alpha_2k_2J_{R0}\varphi^{-1}\mathrm{diag}\left\{|\tilde{q}_{ei}|^{\alpha_2-1}\right\}\varphi\omega_e\\&+2k_1J_{R0}\dot{\varphi}^{-1}\mathrm{sig}^{\alpha_1}\left\{|\tilde{q}_{ei}|^{\alpha_1-1}\right\}+2k_2J_{R0}\dot{\varphi}^{-1}\mathrm{sig}^{\alpha_2}\left\{|\tilde{q}_{ei}|^{\alpha_2-1}\right\}\\&-(\omega_e+A(q_e)\omega_d)^{*}\Delta J_R(\omega_e+A(q_e)\omega_d)\\&+\Delta J_R(\omega_e{}^{*}A(q_e)\omega_d-A(q_e)\dot{\omega}_d)-\Delta J_R\omega_e+u+d\end{aligned}\tag{34}$$

Equation 34 can be derived as follows:

$$J_{0R}\dot{S}_F=G+D+u\tag{35}$$

where G is defined as the known state of the system and D is defined as the unknown state of the system. The function of G and D is written as follows:

$$\begin{aligned}G=&-(\omega_e+A(q_e)\omega_d)^{*}J_0(\omega_e+A(q_e)\omega_d)+J_0(\omega_e{}^{*}A(q_e)\omega_d-A(q_e)\dot{\omega}_d)\\&+\alpha_1k_1J_0\varphi^{-1}diag\left\{|\tilde{q}_{ei}|^{\alpha_1-1}\right\}\varphi\omega_e+\alpha_2k_2J_0\varphi^{-1}diag\left\{|\tilde{q}_{ei}|^{\alpha_2-1}\right\}\varphi\omega_e\\&+2k_1J_0\dot{\varphi}^{-1}\mathrm{sig}^{\alpha_1}\left\{|\tilde{q}_{ei}|^{\alpha_1-1}\right\}+2k_2J_0\dot{\varphi}^{-1}\mathrm{sig}^{\alpha_2}\left\{|\tilde{q}_{ei}|^{\alpha_2-1}\right\}\end{aligned}\tag{36}$$

$$\begin{aligned}D=&-(\omega_e+A(q_e)\omega_d)^{*}\Delta J(\omega_e+A(q_e)\omega_d)\\&+\Delta J(\omega_e{}^{*}A(q_e)\omega_d-A(q_e)\dot{\omega}_d)+d-\Delta J\omega_e\end{aligned}\tag{37}$$

We defined $\dot{x}_1=J_0\dot{S}, x_2=D, \dot{x}_2=z$, and Eq. 35 can be further represented as follows:

$$\begin{cases}\dot{x}_1=G+x_2+u\\ \dot{x}_2=z(t)\end{cases}\tag{38}$$

The FxESO is designed as follows:

$$\begin{cases}\dot{y}_1=G+y_2+u+\beta_1\Gamma\mathrm{sig}^{o_1}(x_1-y_1)+\gamma_1(1-\Gamma)\mathrm{sig}^{\zeta_1}(x_1-y_1)\\ \dot{y}_2=\beta_2\Gamma\mathrm{sig}^{o_2}(x_1-y_1)+\gamma_2(1-\Gamma)\mathrm{sig}^{\zeta_2}(x_1-y_1)+\eta\mathrm{sig}(x_1-y_1)\end{cases}\tag{39}$$

y_1 and y_2 are estimates of $J_{0R}S_F$ and D, respectively. $\beta_1, \beta_2, \gamma_1, \gamma_2$, and η are the observation parameters, with $\eta > \max\{z\}$. $o_1 \in (1-\kappa, 1); \zeta_1 \in (1, 1+\kappa); o_2 = 2o_1 - 1; \zeta_2 = 2\zeta_1 - 1$; and κ is a sufficiently small value. The indicator function Γ is designed as follows:

$$\Gamma=\begin{cases}0, t\le T\\ 1 \text{ else}\end{cases}\tag{40}$$

The observation errors are designed as $E_1=x_1-y_1$ and $E_2=x_2-y_2$. Then, the dynamic functions of the observation errors can be written as follows:

$$\begin{cases}\dot{E}_1=E_2-\beta_1\Gamma\mathrm{sig}^{o_1}(E_1)-\gamma_1(1-\Gamma)\mathrm{sig}^{\zeta_1}(E_2)\\ \dot{E}_2=-(\beta_2\Gamma\mathrm{sig}^{o_2}(x_1-y_1)+\gamma_2(1-\Gamma)\mathrm{sig}^{\zeta_2}(x_1-y_1)+\eta\mathrm{sig}(x_1-y_1))+z(t)\end{cases}\tag{41}$$

It can be proved that there exist $\beta_1, \beta_2, \gamma_1$, and γ_2, such that the observation error E_1 converges to 0 in the fixed time T_1, and the observation error E_2 converges to a small value χ within a fixed time $t < T_1 + T_2$. The expressions of T_1 and T_2 are written as follows:

$$\begin{cases}T_1\le\dfrac{\max\{H\}}{\min\{P\}}\dfrac{2}{1-o_1}\left(\dfrac{\zeta_1-1}{2}\dfrac{2\min\{P\}}{\max\{H\}T}\right)^{\frac{1-o_1}{1-\zeta_1}}+T\\ T_2\le\dfrac{\chi}{\eta-\max\{z\}}\end{cases}\tag{42}$$

where $H=H^{\mathrm{T}}$ and $P=P^{\mathrm{T}}$, such that $Q^{\mathrm{T}}H+HQ=-P$ and $Q=\begin{bmatrix}-\gamma_1 I_{3\times3} & I_{3\times3}\\ -\gamma_2 I_{3\times3} & 0\end{bmatrix}$.

Proof:

The Lyapunov function can be written as:

$$V_2=\iota^{\mathrm{T}}H\iota\tag{43}$$

where, when $t \le T$, $\iota=\left[\mathrm{sig}(E_1)^{\mathrm{T}}\ \mathrm{sig}^{\frac{1}{\zeta_1}}(E_2)\right]$; when $t > T$, $\iota=\left[\mathrm{sig}(E_1)^{\mathrm{T}}\ \mathrm{sig}^{\frac{1}{o_1}}(E_2)\right]$; and H is defined in Eq. 42. According to [23], it can be proved that:

$$\begin{aligned}\dot{V}_2(1,\iota)=&\dot{\iota}^{\mathrm{T}}H\iota+\iota^{\mathrm{T}}H\dot{\iota}=E^{\mathrm{T}}(Q^{T}H+HQ)E\\=&E^{\mathrm{T}}(-P)E\le0\end{aligned}\tag{44}$$

where, Q and P are defined in Eq. 42. On the basis of [28], we obtain the following:

$$\begin{aligned}V_2(1,\iota)=&\iota^{\mathrm{T}}H\iota\le\max\{H\}\|\iota^2\|\\ \dot{V}_2(1,\iota)=&E^{\mathrm{T}}(-P)E\le-\min\{P\}\|\iota^2\|\end{aligned}\tag{45}$$

Then, the Eq. 45 can be written as:

$$\dot{V}_2(1,\iota) \le -\frac{\max\{\boldsymbol{H}\}}{\min\{\boldsymbol{P}\}}\boldsymbol{V}_2(1,\iota) \tag{46}$$

Moreover, according to [23], Eq. 46 can be written as:

$$\dot{V}_2 \le \begin{cases} -\dfrac{\max\{\boldsymbol{H}\}}{\min\{\boldsymbol{P}\}} V_2^{\frac{1+\zeta_1}{2}}(\varsigma_1,\iota), t \le T \\ -\dfrac{\max\{\boldsymbol{H}\}}{\min\{\boldsymbol{P}\}} V_2^{\frac{1+o_1}{2}}(o_1,\iota), t > T \end{cases} \tag{47}$$

When $t = T$, $V_2(\varsigma_1,\iota)$is satisfied as:

$$V_2(\varsigma_1,\iota) \le \left(\frac{\zeta_1 - 1}{2}\frac{\min\{\boldsymbol{P}\}}{\max\{\boldsymbol{H}\}}T\right)^{\frac{2}{1-\zeta_1}} \tag{48}$$

As $o_1 \in (1-\kappa, 1)$, $V_2(\varsigma_1,\iota)$is limited of $V_2(o_1,\iota)$. Then, the observation error converges to 0 within fix time.

Design of the spacecraft control law

On the basis of the FNTSM and FxESO, the controller of the spacecraft is designed as follows:

$$\boldsymbol{u} = -\left(k_3 \mathrm{sig}^{\alpha_3}(\boldsymbol{S_F}) + k_4 \mathrm{sig}^{\alpha_4}(\boldsymbol{S_F}) + k_5 \boldsymbol{S_F} + \boldsymbol{y}_2 + \boldsymbol{G}\right) \tag{49}$$

where the parameters $k_3, k_4, k_5 > 0$; $\alpha_3 > 1$; $0 < \alpha_4 < 1$; $\boldsymbol{S}_F$ is the FNTSM surface in Eq. 24; $\boldsymbol{y}_2$ are estimates of $\boldsymbol{D}$ in Eq. 39; and $\boldsymbol{D}$ and $\boldsymbol{G}$ are defined in Eqs. 36 and 37.

Proof:

Taking $V_3 = \frac{1}{2}\boldsymbol{S}_F^{\mathrm{T}}\boldsymbol{J}_{R0}\boldsymbol{S}_F$ as the Lyapunov function, the derivative of V_3 is derived as follows:

$$\dot{V}_3 = \frac{1}{2}\boldsymbol{S}_F^{\mathrm{T}}\boldsymbol{J}_{R0}\boldsymbol{S}_F = \frac{1}{2}\boldsymbol{S}_F^{\mathrm{T}}\left(-k_3 \mathrm{sig}^{\alpha_3}(\boldsymbol{S_F}) - k_4 \mathrm{sig}^{\alpha_4}(\boldsymbol{S_F}) - k_5 \boldsymbol{S_F} - \boldsymbol{y}_2 + \boldsymbol{x}_2\right) \tag{50}$$

We define $\boldsymbol{E} = \left[\boldsymbol{E}_1^{\mathrm{T}} \ \boldsymbol{E}_2^{\mathrm{T}}\right]^{\mathrm{T}}$ as the observation error matrix. Then, it can be proofed that:

$$\boldsymbol{S}_F^{\mathrm{T}}\left(-\boldsymbol{y}_2 + \boldsymbol{x}_2\right) \le |\boldsymbol{S_F}||\boldsymbol{E}| \tag{51}$$

The Eq. 50 can further derived as follows:

$$\begin{aligned} \dot{V}_3 &\le -k_3 \boldsymbol{S}_F^{\mathrm{T}} \mathrm{sig}^{\alpha_3}(\boldsymbol{S_F}) - k_4 \boldsymbol{S}_F^{\mathrm{T}} \mathrm{sig}^{\alpha_4}(\boldsymbol{S_F}) - k_5 \boldsymbol{S}_F^{\mathrm{T}} \boldsymbol{S_F} + |\boldsymbol{S_F}||\boldsymbol{E}| \\ &\le -k_4 3^{\frac{1-\alpha_3}{2}} \left(\frac{2}{\max\{\boldsymbol{J}_{R0}\}}\right) V_3^{\frac{\alpha_3+1}{2}} - k_5 3^{\frac{1-\alpha_4}{2}} \left(\frac{2}{\max\{\boldsymbol{J}_{R0}\}}\right) V_3^{\frac{\alpha_4+1}{2}} \end{aligned} \tag{52}$$

Therefore, it can be proved [27] that the controller achieves convergence and stability in fix time.

Results and Discussion

Cantilevered film simulation

In this section, a cantilevered film example is presented to demonstrate the performance of the ANCF shell element developed in this paper. The 2 corners at one end of the rectangular cantilever membrane are hinged and constrained, and the other end swings under gravity, as shown in Fig. 6. The length, width, and thickness of the plate are assumed to be 1.0, 1.0, and 0.005 m, respectively. The Young's modulus and Poisson's ratio are assumed to be 1.24×10^7 Pa and 0.3, respectively. The cantilevered film example is modeled and simulated using ANCF elements and S4 shell elements in ABAQUS, respectively.

As shown in Fig. 7, the curve of ANCF_elements10 * 10 is relatively close to the curve of ANCF_elements20 * 20. Therefore, the film only needs to be divided into $10 \times 10 = 1000$ ANCF elements to achieve convergence of mesh division. In addition, as shown in Fig. 8, the curve of ABAQUS_elements30 * 30 is relatively close to the curve of ABAQUS _elements50 *50, indicating that 900 elements need to be divided to ensure the accuracy of the ABAQUS results. Because of the high degree of freedom of the ANCF element, the convergence of the element is much better than the shell element in ABAQUS. In addition, as shown in Fig. 9, the overall trend of the calculation results of ANCF element and ABAQUS shell element is consistent, which verified the correctness of the ANCF element.

Virtual prototype of the spacecraft with film capture pocket system

On the basis of the dynamics and controller theory, a virtual prototype of the service spacecraft with a film capture pocket system is established as shown in Fig. 10. The service spacecraft dynamic system mainly contains film surface dynamic model, flexible rod dynamic model, and spacecraft attitude dynamic model. The dynamic system simulates the attitude angle $\boldsymbol{q}$, the deformation state of the large flexible parts, the interaction force between the film capture pocket and the spacecraft body, and other dynamic properties in real time. The attitude control system of the spacecraft system is mainly composed of FNTSM and FxESO. The simulation process of dynamics and control of the spacecraft with film capture pocket system is as follows: First, the attitude error quaternion $\boldsymbol{q}_e$ is calculated on the basis of the motion state $\boldsymbol{q}$ of the dynamical system in real-time feedback. Second, the control system provides the FNTSM function and FxESO function respectively based on the attitude error $\boldsymbol{q}_e$. The controller $\boldsymbol{u}$ of the spacecraft system is calculated according to Eq. 49. Finally, the service spacecraft dynamic system calculates the system motion state $\boldsymbol{q}$. Then, the closed-loop simulation of the whole virtual prototype is completed.

Design of simulation parameters

The controller parameters are designed in Table 1.

The maximum diameter of the capture system is 4.12 m, and the maximum depth is 4 m. The diameter of each flexible rod is 0.1 m, the thickness of film surface is 3 mm, and the others are as shown in Fig. 11. The film capture pocket system is divided into ANCF elements mesh, as shown in Fig. 11.

The dynamic parameters of the service spacecraft are designed in Table 2.

The material properties of film surface and flexible rods are in Table 3.

Analysis of simulation results

On the basis of the virtual prototype, the attitude maneuver process of the system is simulated as shown in Fig. 12. As the spacecraft attitude stabilizes, the oscillation of the flexible rod decreases, and the overall system tends to stabilize. However, because of the low stiffness of the flexible rods, the flexible rod could not completely tension the film surface. The folds of the film persisted for a long time and could not be completely restored to a flat state. The spacecraft undergoes large

controller converges at about 35 s. The comparison of convergence time shows that the FNTSM + FxESO controller substantially improves the convergence speed of the system attitude errors.

Figure 18 shows the FNTSM + FxESO torque input *u* curves. There is no obvious chattering for the control torque due to the compensation of the observer for the unknown disturbances in the system. During 0 to 10 s, the torque input is large because the attitude error of the system is large in the initial state. After 10 s, the attitude tracking error of the system gradually converges, and the control torque also decreases. However, because of the vibration of the flexible film capture pocket, there is also a slight vibration of the control torque. In addition, the control torque is not constant to 0.

Conclusion

1. A new film capture pocket system is proposed in this paper to solve the space debris problems. The film structure effectively avoids the structure self-tangling while also preventing the capture target from escaping.
2. The film dynamic model is established on the basis of high-order ANCF theory. It was verified that the high-order ANCF element has better convergence than the ABAQUS shell element.
3. A complex service spacecraft dynamic simulation system is developed. The simulation results show that the vibration of the flexible capture mechanism causes large nonlinear disturbances to the spacecraft.
4. The FNTSM + FxESO controller is designed. The steady-state attitude error of the spacecraft is 10^{-4} order of magnitude. There is no obvious chattering of attitude torque input. The attitude error under the FNTSM + FxESO control law converges faster, compared with NTSM+ESO control law. These simulation results indicate the effectiveness and stability of the controller.

Moreover, the research in this paper is limited to a simulation environment. There are maybe some foreseen challenges if the proposed control law is to be realized on a physical system, for example, sensor sampling frequency limitations, saturation of spacecraft actuator outputs, control system delays, etc. Subsequent studies will further refine the theoretical approach of this paper in conjunction with physical experiments.

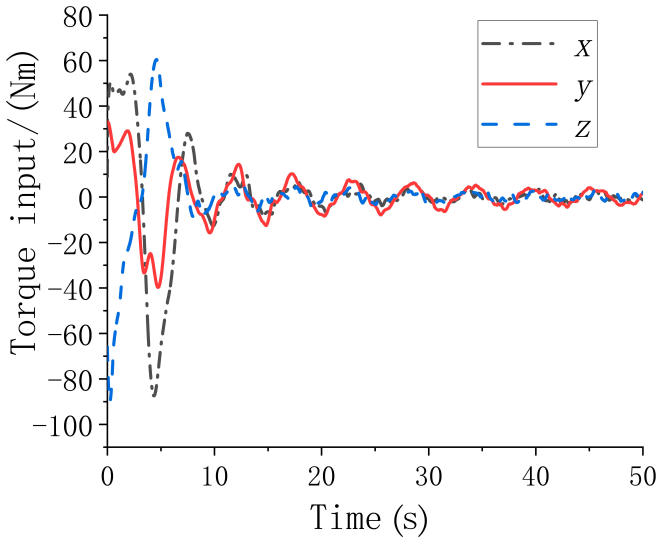

Fig. 18. Torque input ***u*** curves.

Acknowledgment

Funding: This research was supported by the Heilongjiang Province Natural Science Foundation (grant number: JJ202-2LH0315) and Postdoctoral Scientific Research Development Fund of Heilongjiang Province (grant number: LBH-Z21141).
Author contributions: This article is co-authored by the 5 authors. Z.H. mainly completes dynamic modeling and simulation. C.T. is responsible for the research and simulation of the controller. Q.Y. analyzed the research background of the article and designed the research object. M.S.S.K. provided support for the writing of the article and the theory of dynamics. C.W. provided software programming support for algorithm solving.
Competing interests: The authors declare that they have no competing interests.

Data Availability

All relevant data are within the paper.

References

1. Pu H, Guangwei W, Yingkai C, Zhaokui W. Reduction of space debris collision prediction uncertainty based on Q-Sat precise orbit. *Space: Sci Technol*. 2023;3:0005.
2. Wang Q, Jin D, Rui X. Dynamic simulation of space debris cloud capture using the tethered net. *Space: Sci Technol*. 2021;2021:Article 9810375.
3. Escalona JL, Hussien HA, Shabana AA. An absolute nodal coordinate formulation for the dynamic analysis of flexible multibody systems. In: Zobel R, Moeller D, editors. *Simulation: Past, present and future*. San Diego (CA): Society for Computer Simulation; 1998. pp. 571–576.
4. Shabana AA, Yakoub RY. Three dimensional absolute nodal coordinate formulation for beam elements: Theory. *J Mech Des*. 2000;123(4):606–613.
5. Simo J, Vuquoc L. On the dynamics in space of rods undergoing large motions - A geometrically exact approach. *Comput Methods Appl Mech Eng*. 1988;66(2):125–161.
6. Hodges DH, Yu W, Patil MJ. Geometrically-exact, intrinsic theory for dynamics of moving composite plates. *Int J Solids Struct*. 2009;46(10):2036–2042.
7. Luo K, Liu C, Tian Q, Hu H. An efficient model reduction method for buckling analyses of thin shells based on IGA. *Comput Methods Appl Mech Eng*. 2016;309:243–268.
8. Nguyen-Xuan H, Tran LV, Thai CH, Kulasegaram S, Bordas SPA. Isogeometric analysis of functionally graded plates using a refined plate theory. *Compos Pt B-Eng*. 2014;64:222–234.
9. Ding J, Wallin M, Wei C, Recuero AM, Shabana AA. Use of independent rotation field in the large displacement analysis of beams. *Nonlin Dynam*. 2014;76(3):1829–1843.
10. Shabana AA. Flexible multibody dynamics: Review of past and recent developments. *Multi Syst Dyn*. 1997;1(2):189–222.
11. Gan BS. Isogeometric analysis of Euler-Bernoulli beam element. *J Adv Civil Environ Engineering*. 2018;2.